Neutron-spectroscopic studies of the crystal field in $ErBa_2Cu_3O_x$ $(6 \leq x \leq 7)$

J. Mesot,* P. Allenspach, U. Staub, and A. Furrer
Eidgenössische Technische Hochschule Zürich, Laboratory for Neutron Scattering, CH-5232 Villigen PSI, Switzerland

H. Mutka
Institut Laue-Langevin, 156 X, F-38042 Grenoble CEDEX, France

R. Osborn and A. Taylor
Rutherford Appleton Laboratory, Didcot, Oxon, United Kingdom
(Received 1 June 1992)

Inelastic neutron scattering has been employed to study in detail the full crystalline-electric-field (CEF) energy scheme in the ground-state J multiplet of Er^{3+} in $ErBa_2Cu_3O_x$ as a function of the oxygen content x. We have been able to resolve the seven ground-state transitions for a series of samples covering the superconducting phase as well as the semiconducting one. J-mixing and intermediate-coupling effects as well as geometrical considerations are shown to be necessary to determine unambiguously the nine CEF parameters of the orthorhombic symmetry. The large energy shifts and intensity changes of the observed CEF spectra as a function of the oxygen content x are shown to be related predominantly to a charge-transfer process from the chains to the planes, the actual charge transfer being in excellent agreement with results derived from bond-valence-sum considerations of diffraction data. The CEF parameters are also used to calculate the magnetization and the field-dependent Schottky anomaly of the heat capacity, which yields remarkable agreement with the experimental data. A mean-field calculation allows us to estimate the x dependence of the saturated moment of the Er^{3+} ion in the ordered phase, which perfectly agrees with the results obtained by means of Mössbauer measurements, but considerably deviates from diffraction values.

I. INTRODUCTION

In the perovskite-type compounds $YBa_2Cu_3O_x$ (1:2:3) $(6<x<7)$ it is well known that the replacement of the Y ions by most of the magnetic rare-earth (R) ions does not have a detrimental effect on superconductivity,[1] in contrast to conventional superconductors. In most cases the oxygen stoichiometry has been shown to have drastic influences on the physical properties of these compounds. As the oxygen content x decreases from 7 to 6, the 1:2:3-type systems show structural transitions, changes in the superconducting transition temperature T_c (two-plateau structure of T_c), as well as a metal to semiconductor transition. For R substituted compounds, at temperatures below 3 K, transitions to two- and three-dimensional antiferromagnetic order of the R ion sublattice have been reported. Despite extensive studies performed by means of several techniques such as magnetic[2] and transport measurements,[3] photoemission spectroscopy,[4] and neutron diffraction,[5] the detailed understanding of the relation between the above-mentioned phase transitions and superconductivity remains controversial.

In this work we propose a different approach based on the analysis of the energetic level splitting of the ground-state J multiplet of the R ion as a function of oxygen content x. In the 1:2:3 compounds the R ions are sandwiched between two superconducting copper-oxide planes. The $(2J+1)$-fold degeneracy of the ground-state J multiplet of the R ion will be partially lifted under the action of the crystalline-electric-field (CEF) potential

$$V_{\mathrm{CEF}}(\mathbf{r}) = \sum_i \frac{Z_i e |e|}{|\mathbf{r}-\mathbf{R}_i|} , \tag{1}$$

where $Z_i e$ denotes the charge at the site $\mathbf{R}_i$ of the ith ligand ion and e is the electronic charge. Equation (1) implies that the CEF energy-level scheme is a direct function of both the structural (denominator) and the charge distribution (numerator) parameters in the vicinity of the R ion. Thus, any modification of the environment of the R ion will significantly affect its energy-level scheme, i.e., the CEF offers a good opportunity and a very clean way to look at the properties of the superconducting planes in the 1:2:3 compounds under various conditions (oxygen deficiency, external pressure, Zn or Ni doping of the Cu sites, irradiation, etc.).

Since very detailed information about the CEF interaction can be obtained from inelastic neutron-scattering (INS) experiments, considerable effort has been involved to study the $RBa_2Cu_3O_x$ systems by means of this technique.[6-9] In this paper we present INS experiments on $ErBa_2Cu_3O_x$ $(6<x<7)$. In these compounds the Er^{3+} ions have a total angular momentum $J=\frac{15}{2}$. The CEF will split the 16-fold degeneracy of the ground-state multiplet $^4I_{15/2}$ into eight Kramers doublets. We have measured for several oxygen concentrations x all seven ground-state CEF transitions (energies and intensities) and in addition some excited-state CEF transitions. The observed energies and intensities are used to determine the CEF potential. This is a complicated task, since, first,

the low symmetry at the rare-earth site (tetragonal for $x \leq 6.4$ and orthorhombic for $x \geq 6.4$) renders difficult a unique determination of the five and nine independent CEF parameters, respectively. To overcome this problem we make use of geometrical coordination considerations. Second, the large overall CEF splitting of these compounds makes it necessary to take into account intermediate coupling as well as J-mixing effects in our calculations. It was then possible to determine a unique set of CEF parameters for each oxygen content. In order to check the reliability of this procedure, our results are used to calculate various thermodynamic magnetic properties of $ErBa_2Cu_3O_x$, which are found to be in excellent agreement with the experimental data.

Significant changes have been observed in the CEF parameters as a function of oxygen content x, which cannot be related to structural changes alone. These changes, however, can be explained by introducing the concept of charge transfer from the chains to the planes. Using an effective point-charge model, a quantitatively good agreement is obtained with bond valence sum arguments,[10] and confirmation is given that the change of T_c is directly connected to the amount of charge being transferred to the planes.

II. EXPERIMENT

The polycrystalline single-phase starting material of $ErBa_2Cu_3O_7$ was prepared by a standard sintering procedure. We treated the powdered material by a temperature controlled oxygen desorption-absorption procedure to yield final oxygen contents of $x = 6.09$, 6.34, 6.45, 6.53, 6.78, 6.91, and 6.98. Each sample was characterized by means of both dc magnetic susceptibility and neutron-diffraction techniques. The samples show the well known two-plateau structure of T_c (Fig. 1),[11] and neutron-diffraction experiments proved the single-phase character of the samples. Only the samples with $x = 6.09$ and 6.34 turned out to be nonsuperconducting. The structure investigations were performed at the reactor Saphir at Würenlingen (Switzerland) with use of a double-axis multi-counter diffractometer. The structural results are listed in Table I.

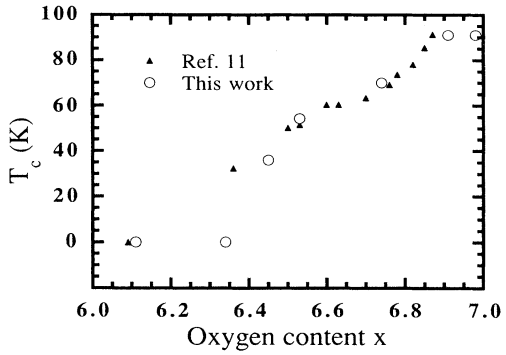

FIG. 1. Superconducting transition temperature T_c vs oxygen content x for $ErBa_2Cu_3O_x$.

The low-energy transfer ($\Delta E < 15$ meV) INS experiments were performed with use of the time-of-flight (TOF) spectrometers IN5 and IN4 at the high-flux reactor of the Institut Laue-Langevin (ILL) at Grenoble with incident neutron energies of 3.27 and 17.21 meV, respectively. We achieved an instrumental resolution (full width at half maximum) of 0.15 meV at $\Delta E = 0.4$ meV on IN5 and, using a very good collimation, 0.4 meV at $\Delta E = 10$ meV on IN4. The $ErBa_2Cu_3O_x$ powdered samples were enclosed into cylindrical aluminum containers of 10 mm diameter and 50 mm height. The high-energy transfer ($50 < \Delta E < 100$ meV) INS experiments were per-

TABLE I. Structural parameters of $ErBa_2Cu_3O_x$ derived in the present work.

Atom	Parameter	6.98	6.91	6.78	6.53	6.45	6.34	6.09
	T (K)	RT	10	RT	RT	RT	10	10
Er	B (Å^2)	0.36(7)	0.26(6)	0.49(7)	0.47(6)	0.56(5)	0.28(8)	0.22 (6)
Ba	B (Å^2)	0.45(7)	0.15(6)	0.45(7)	0.43(7)	0.59(5)	0.24(9)	0.15(7)
	Z	0.1842(3)	0.1830(3)	0.1868(3)	0.1891(2)	0.1904(2)	0.1932(3)	0.1948(3)
Cu(1)	B (Å^2)	0.56(8)	0.23(6)	0.91(9)	0.88(7)	0.73(5)	0.27(8)	0.36(6)
Cu(2)	B (Å^2)	0.28(5)	0.05(5)	0.23(5)	0.29(4)	0.45(3)	0.07(5)	0.08(4)
	Z	0.3561(2)	0.3559(2)	0.3577(2)	0.3586(2)	0.3600(2)	0.3612(3)	0.3618(2)
O(1)	B (Å^2)	0.56(8)	0.270(6)	0.86(9)	0.96(7)	1.29(5)	0.59(8)	0.81(8)
	Z	0.1587(3)	0.1586(3)	0.1568(3)	0.1551(3)	0.1548(3)	0.1542(4)	0.1530(3)
O(2)	B (Å^2)	0.52(5)	0.270(6)	0.68(5)	0.75(5)	0.63(5)	0.17(7)	0.14(5)
	Z	0.3798(4)	0.3800(3)	0.3804(4)	0.3803(4)	0.3805(3)	0.3798(6)	0.3798(8)
O(3)	B (Å^2)	0.52(5)	0.14(6)	0.68(5)	0.75(5)	0.91(5)		
	Z	0.3780(4)	0.3781(3)	0.3783(4)	0.3785(4)	0.3783(3)		
O(4)	B (Å^2)	2.1(3)	2.1(4)	2.3(4)	2.5(4)	2.1(3)	1.9(5)	1.8(3)
	n (%)	98(2)	91(2)	78(2)	53(2)	45(2)	34(2)	9(2)
	a (Å)	3.8213(2)	3.8140(2)	3.8259(2)	3.8354(2)	3.8379(1)	3.8452(6)	3.8500(5)
	b (Å)	3.8876(2)	3.8794(2)	3.8861(2)	3.8788(2)	3.8697(1)		
	c (Å)	11.6955(8)	11.6899(7)	11.7197(8)	11.7510(6)	11.7558(6)	11.7643(8)	11.7878(7)
	Rp	3.03	8.99	3.12	2.45	5.54	3.11	2.55
	Rwp	3.89	9.19	3.97	3.29	7.4	3.88	3.21
	Rex	1.28	3.19	1.83	0.9	2.78	1.91	1.14
	RF	2.89	3.32	3.19	3.62	6.57	3.53	3.40

formed with the use of the TOF spectrometer HET at the spallation neutron source ISIS of the Rutherford Appleton Laboratory at Didcot. We used an incident energy of 100 meV in order to achieve an instrumental resolution of less than 2 meV at $\Delta E = 80$ meV. The $ErBa_2Cu_3O_x$ powdered samples were filled into a rectangular aluminum container of $65 \times 65 \times 5$ mm^3 volume. All the experiments were performed in the temperature range from 10 to 100 K using a conventional helium cryostat. The raw data have been corrected for absorption, detector efficiency, and background effects using standard procedures.

III. RESULTS

A. $ErBa_2Cu_3O_{6.98}$

The energy spectra taken at $T = 10$ K exhibit seven inelastic lines, which are considerably separated in energy: We observe three inelastic lines A, B, C in a low-energy window ($\Delta E < 12$ meV) and four inelastic lines D,E,F,G in a high-energy window ($65 < \Delta E < 82$ meV) as shown in Figs. 2(b) and 2(c). The gap between the two windows is structureless. There is no doubt about the magnetic origin of these inelastic lines, since the intensities observed for the reference sample $YBa_2Cu_3O_7$ turned out to be at least one order of magnitude smaller in these two energy windows. A more detailed understanding of the observed energy spectra is obtained by considering the differential neutron cross section for the CEF transition $|\Gamma_n\rangle \longrightarrow |\Gamma_m\rangle$, which is given in the dipole approximation by[12]

$$\frac{\partial^2\sigma}{\partial\Omega\partial\omega} = \frac{N}{Z}\left[\frac{\gamma e^2}{m_e c^2}\right]^2 \frac{k_1}{k_0}\exp\{-2W(\mathbf{Q})\}F^2(\mathbf{Q}) \times \exp\left[\frac{-E_n}{k_B T}\right]|\langle\Gamma_m|J_\perp|\Gamma_n\rangle|^2\delta(E_m - E_n + h\omega)\,. \quad (2)$$

Z is the partition function, $F(\mathbf{Q})$ the magnetic form factor, E_n the energy of the nth CEF state with irreducible representation Γ_n, and $J_\perp$ the component of the total angular momentum operator perpendicular to the scattering vector $\mathbf{Q}$. The remaining symbols have their usual meaning. We should note that in the case of Er^{3+}, $\langle\Gamma_m|J_\perp|\Gamma_n\rangle \neq 0$ for all n and m, which gives us the possibility to observe all the CEF transitions. It follows from Eq. (2) that the intensities of the CEF transitions are governed by Boltzman statistics, and they are decreasing with increasing modulus of the scattering vector $\mathbf{Q}$ due to the form factor, in contrast to phonon intensities, which usually increase with $|\mathbf{Q}|$ and temperature (Bose statistics). Figure 3 shows the temperature and $\mathbf{Q}$ dependence of the low-energy transitions of the $x = 6.98$ compound. The intensities decrease by 50% when raising the temperature from 10 to 100 K as expected from the Boltzman factor. We observe a decrease of 25% between the low-Q ($\langle Q_L\rangle = 0.8$ Å^{-1}) and the high-Q ($\langle Q_H\rangle = 2.4$ Å^{-1}) data, in excellent agreement with magnetic form factor calculations using the values tabulated by Freeman and Desclaux.[13] A similar behavior was observed for the high-energy transitions. We can thus interpret all seven lines A–G in terms of CEF transitions out of the ground state, since at low temperature only the CEF ground state is populated. The high-energy window (Fig. 4) is slightly more complicated, since with increasing temperature new peaks are appearing between 55 and 75 meV, which correspond to a superposition of 12 *inter*window transitions between the low-energy and the high-energy CEF states. At the same time the ground-state intensities of the transitions D, E, F, G decrease with increasing temperature. Figure 2(a) shows *intra*window transitions between the states A,B,C. As explained in the following, all these transitions (energies as well as relative intensities) have been considered for the determination of the CEF parameters.

B. Dependence upon oxygen concentration x

Figure 5 shows the oxygen stoichiometry dependence of the observed energy spectra. When going from $x = 6$

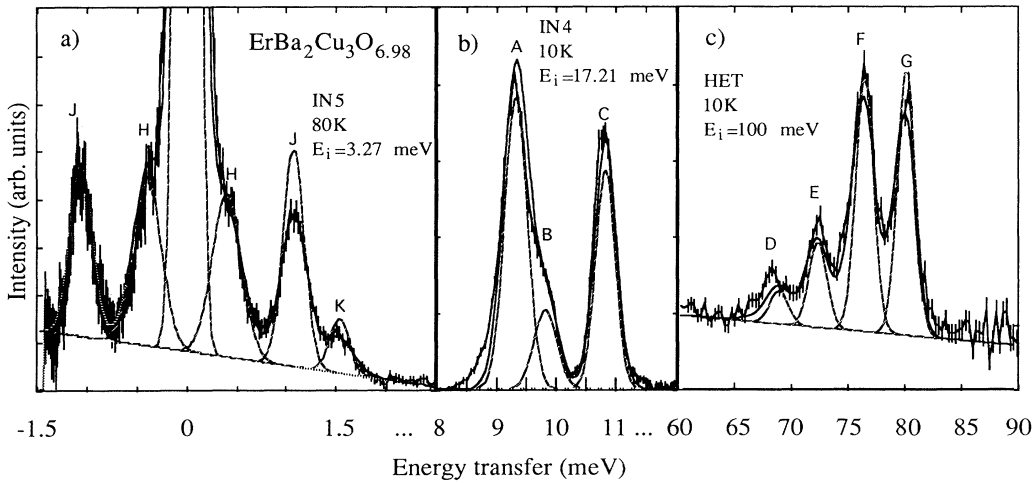

FIG. 2. Energy spectra of neutrons scattered from $ErBa_2Cu_3O_{6.98}$. The solid lines represent the calculated spectra, which result from a convolution of the intrinsic Gaussian functions (dashed lines) with the instrumental resolution function.

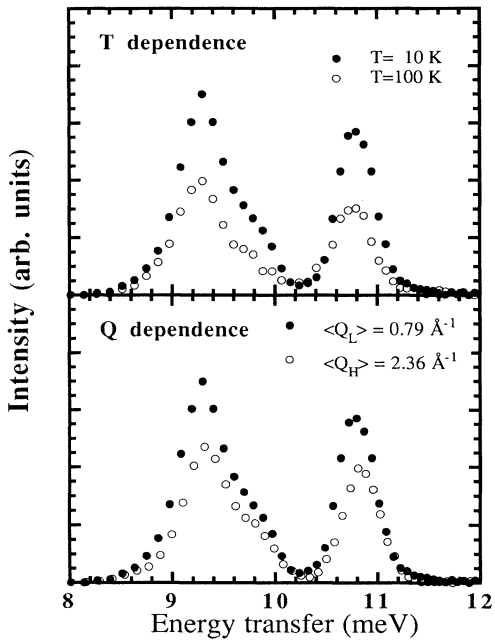

FIG. 3. Temperature and Q dependences of the IN4 data taken for $ErBa_2Cu_3O_{6.98}$ ($E_i = 17.21$ meV).

to $x = 7$, the transitions B,D,E shift slightly to lower energies, and the transitions A,F,G move up to higher energies, whereas the energy of the transition C remains unchanged. Note that the linewidth of the transitions B,C,D,E,F,G is a monotonic function of x, in contrast to the linewidth of the transition A, which shows an interesting behavior. It is very well defined for $x = 6.98$, $x = 6.53$, and $x = 6.09$, while it is much more broadened for the other concentrations x. In the data analysis we simply considered the center of gravity and the integrated intensity of each peak. In order to reduce the number of parameters we assumed a linear energy dependence of the intrinsic linewidth. We then convoluted the intrinsic function (Gaussian) with the instrumental resolution function, in order to compare the calculated energy spectra with the experimental data.

IV. CRYSTAL-FIELD CALCULATION

The degeneracy of the J multiplets of a magnetic ion embedded in a crystal lattice is partly removed by the CEF potential produced by the charge distribution of the surrounding ions. The corresponding CEF potential at the R sites takes the form given by Eq. (1). Using the tensor operator equivalents method we can construct the following Hamiltonian:

$$H_{\mathrm{CEF}} = \sum_{n=1}^{3} \sum_{m=0}^{n} A_{2n}^{2m} Y_{2n}^{2m} , \tag{3}$$

where the Y_{2n}^{2m} are spherical tensor operators[14] and the A_{2n}^{2m} denote the CEF parameters.

Usually the CEF potential is treated as a perturbation of the ground-state multiplet $^{2S+1}L_J$ alone. For the present case this approximation is not able to yield parameters that correctly reproduce the observed energies and intensities, since the overall CEF splitting of the $ErBa_2Cu_3O_x$ compounds (~ 100 meV) is comparable in magnitude to the intermultiplet splitting energies (~ 800 meV for Er^{3+}). This leads to a mixing of the different J multiplets through the CEF interaction (J mixing). Furthermore, due to the spin-orbit coupling, S and L are no longer good quantum numbers. Indeed every J multiplet is contaminated by states of different L, S but same J (intermediate coupling). Therefore, in the present investigation we have performed a simultaneous diagonalization of the electrostatic, spin-orbit, and crystal-field interactions. The Hamiltonian is now written

$$H = H_{\mathrm{EL}} + H_{\mathrm{SO}} + H_{\mathrm{CEF}} , \tag{4a}$$

with

$$H_{\mathrm{EL}} = \sum_{k=0}^{3} E^k e_k , \tag{4b}$$

$$H_{\mathrm{SO}} = \xi A_{\mathrm{so}} . \tag{4c}$$

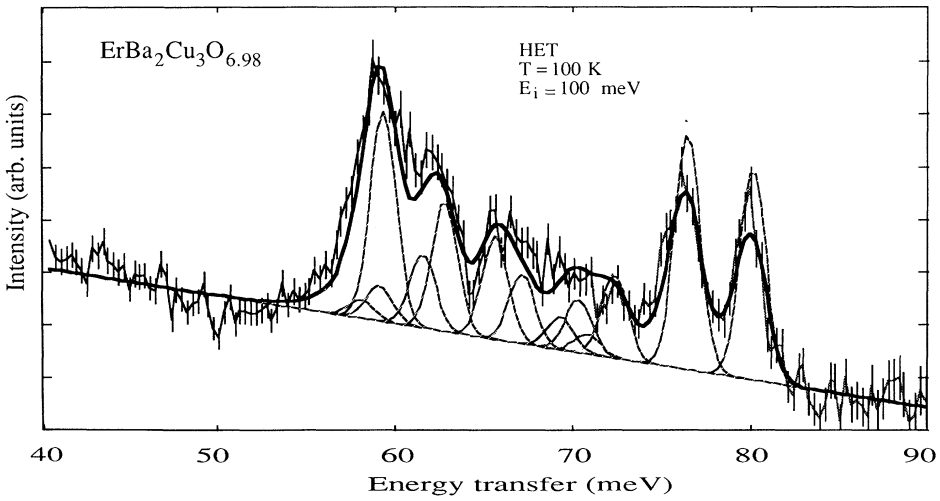

FIG. 4. High-temperature ($T = 100$ K) energy spectrum of neutrons scattered from $ErBa_2Cu_3O_{6.98}$ taken at HET. $E_i = 100$ meV. The lines are as in Fig. 2.

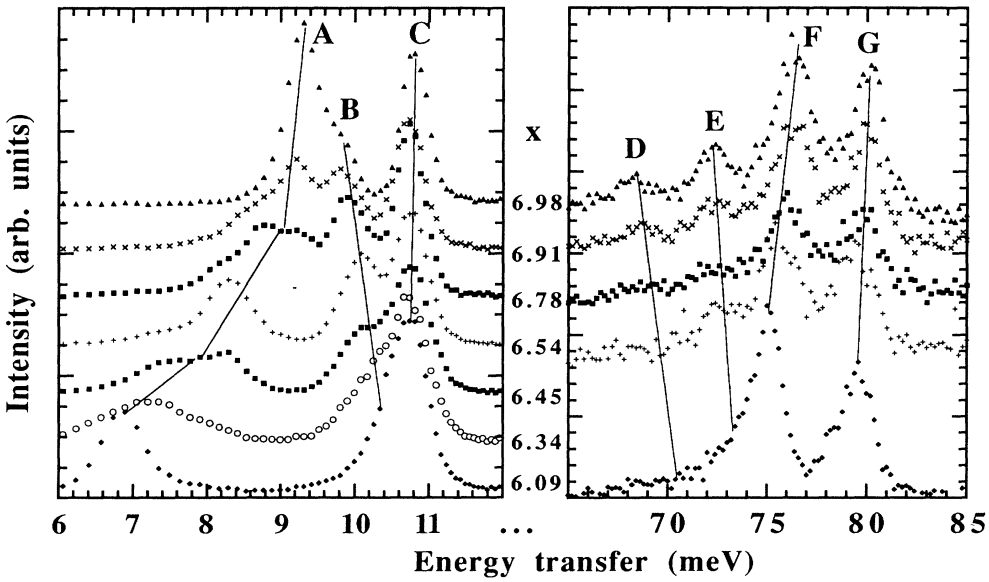

FIG. 5. Energy spectra obtained for $ErBa_2Cu_3O_x$ at $T=10$ K taken at IN4 (left part, $E_i=17.2$ meV) and HET (right part, $E_i=100$ meV). The lines indicate the x dependence of the observed ground-state transitions.

The adjustable free ion parameters E^k and ξ correspond to Slater electrostatic and spin-orbit integrals, respectively; they have been taken from Wybourne.[16] e_k and A_{so} represent matrix elements for the angular parts of these electrostatic and spin-orbit interactions, which have been tabulated by Nielson and Koster.[17] In the case of $ErBa_2Cu_3O_x$ J-mixing and intermediate coupling effects are similar in magnitude (note that these two effects enhance the separation between the low-energy and high-energy window), and all together they produce changes of the order of 5% in the CEF energy-level scheme (Fig. 6). This is far outside our experimental accuracy, thus all the multiplets with $J=\frac{15}{2}$, $\frac{13}{2}$ and $\frac{11}{2}$ have been considered in our calculations.

The energies and intensities of the seven CEF ground-state transitions A–G have been considered for the fitting of the CEF parameters. Although this is sufficient to determine unequivocally all five CEF parameters of the tetragonal phase, some more information is needed to achieve a unique determination of the nine orthorhombic CEF parameters. In order to solve this problem we used the following procedure for the two extreme concentra-

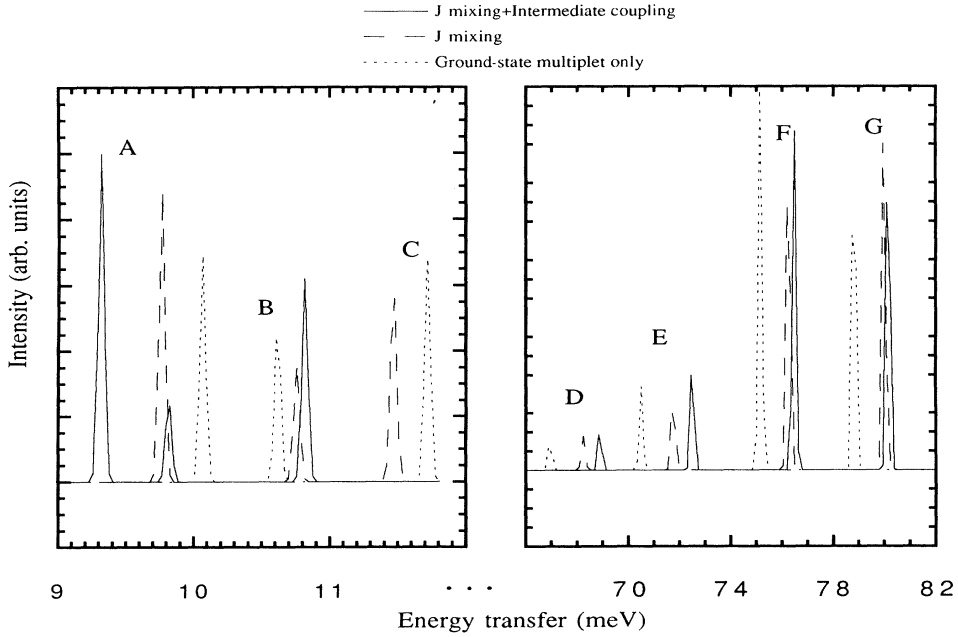

FIG. 6. Influence of J mixing and intermediate coupling on the energy spectrum of $ErBa_2Cu_3O_{6.98}$.

tions $x=6.09$ and $x=6.98$. In the point-charge approximation, the CEF parameters are explicitly given by:

$$A_{2n}^{2m}=e|e|\langle r^{2n}\rangle \sum_i Z_i \gamma_{2n}^{2m}(i) , \tag{5a}$$

with

$$\gamma_{2n}^{2m}(i)=\frac{f_{2n}^{2m}(\theta_i,\phi_i)}{(\mathbf{r}-\mathbf{R}_i)^{2n+1}} . \tag{5b}$$

The sum i runs over all neighboring ions at position $\mathbf{R}_i=(R_i,\theta_i,\phi_i)$, $\sqrt{4\pi/(4n+1)}f_{2n}^{2m}(\theta_i,\phi_i)$ are tesseral harmonics, $\langle r^{2n}\rangle$ is the $2n$th moment of the radial distribution of the $4f$ electrons, Z_i is the charge of the ith ion in units of the electron charge $|e|$, and $\gamma_{2n}^{2m}(i)$ are the geometrical coordination factors as defined, e.g., by Hutchings.[15] For tetragonal symmetry the parameters with $m=1$ and $m=3$ vanish. In a first step we considered a model with only three independent CEF parameters A_2^0, A_4^0, A_6^0, whereas the remaining CEF parameters were fixed at their geometric coordination values:

$$A_{2n}^{2m}=A_{2n}^{0}\gamma_{2n}^{2m}(\mathrm{O}(2),\mathrm{O}(3))/\gamma_{2n}^{0}(\mathrm{O}(2),\mathrm{O}(3)) . \tag{6}$$

The coordination factors γ_{2n}^{2m}, Eq. (5b), were calculated from the nearest-neighbor oxygen polyhedron determined by neutron diffraction. An attempt was made to start with values determined by the nearest-neighbor copper coordination, but this failed totally to provide agreement between observed and calculated intensities. Similar results have been obtained in the case of the $HoBa_2Cu_3O_7$ compound.[18] This is not unexpected, since the large CEF splitting of these systems is very similar to the one observed in the garnet compounds[19] where the CEF splitting has its origin in the eight nearest-neighbor oxygen ligands. Therefore, we can conclude that the CEF interaction in the high-T_c perovskite compounds is mainly governed by the charge distribution of the nearest-neighbor oxygen shell, with the exception of the second-order CEF potential, for which also more distant neighboring coordination shells have to be taken into account. Following Lea, Leask, and Wolf[20] we introduced the parametrization

$$\begin{aligned} B_2^0F_2&=A_2^0\chi_2F_2=W(1-|y|) ,\\ B_4^0F_4&=A_4^0\chi_4F_4=Wxy , \\ B_6^0F_6&=A_6^0\chi_6F_g=W(1-|x|)y , \end{aligned} \tag{7}$$

with $F_2=2$, $F_4=60$, $F_6=13\,860$, $-1\le x,y\le 1$, and W is a scale factor. The χ_n are the reduced matrix elements as tabulated by Hutchings[15] and relate our notation to the CEF parameters B_n^m as used in Ref. 20. Equation (7) corresponds to the most general combination of second-, fourth-, and sixth-order CEF parameters. For only one parameter set x,y reasonable agreement between the observed and calculated energies and intensities was obtained, namely for $x\approx -0.45$ and $y\approx 0.8$. In fact, the observed separation of the CEF states into a low- and high-energy window can only be achieved for $x\approx -0.45$ (see Fig. 1 in Ref. 20).

In the second step of the least-squares fitting procedure, after having determined the most reasonable start values of the diagonal CEF parameters, all the leading "tetragonal" parameters ($m=0,2$) were allowed to vary independently, whereas the remaining "orthorhombic" CEF parameters ($m=1,3$) were still fixed at their geometrical values according to Eq. (6). The procedure converged to a modified set of parameters which, however, deviated by less than 10% from the values obtained in the first step. Thus our parametrization (five independent parameters fitted to seven energies and intensities of ground-state transitions) can undoubtedly be considered to be a unique solution. At this point the procedure was fully satisfying to reproduce all ground-state energies and intensities of the $x=6.09$ sample, since all the orthorhombic parameters are set to zero in the tetragonal case. Nevertheless, in order to obtain a good fit of the $x=6.98$ data, a third step, where all nine parameters were simultaneously refined, was necessary; in this procedure the leading tetragonal parameters remained essentially unchanged, whereas the orthorhombic CEF parameters deviated from the geometrical values by less than a factor of two. In order to test the reliability of our parameters, we calculated the energy spectra for $ErBa_2Cu_3O_{6.98}$ at high temperature where *inter* and *intra*window excited CEF transitions are appearing, which are found to be in good agreement with the experimental data as shown in Figs. 2(a) and 4. The resulting energy level scheme for Er^{3+} in $ErBa_2Cu_3O_{6.98}$ is displayed in Fig. 7.

We then used the final parameters of the $x=6.09$ and $x=6.98$ samples as starting values for the other oxygen concentration samples. The final result does not depend

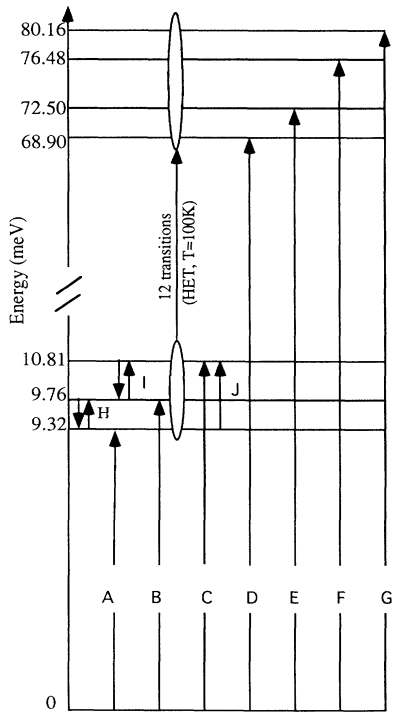

FIG. 7. Observed transitions and resulting CEF level scheme of $ErBa_2Cu_3O_{6.98}$.

TABLE II. CEF parameters A_n^m (in meV) of $ErBa_2Cu_3O_x$ derived in this work. Our notation is related to the Stevens formalism in the following way: $A_n^m = B_n^m/\chi_n$, where χ_n are the reduced matrice elements as tabulated by Hutchings (Ref. 15).

x	A_2^0	A_2^2	A_4^0	A_4^2	A_4^4	A_6^0	A_6^2	A_6^4	A_6^6
6.09	6.30±0.22	0	−33.61±0.11	0	156.31±0.66	3.57±0.02	0	104.47±0.11	0
6.34	7.46±0.20	0	−33.54±0.13	0	156.27±0.59	3.59±0.02	0	104.52±0.10	0
6.45	8.85±0.34	2.48±2.8	−33.22±0.16	3.63±3.3	155.77±0.51	3.64±0.03	−0.11±0.09	104.47±0.16	0.18±0.08
6.53	9.37±0.18	4.81±2.2	−33.14±0.09	4.89±2.2	156.08±0.56	3.66±0.02	−0.25±0.08	104.47±0.08	0.41±0.10
6.78	11.97±0.28	7.74±2.5	−32.41±0.15	8.37±2.1	157.28±0.86	3.68±0.02	−0.48±0.10	104.60±0.11	0.60±0.11
6.91	12.59±0.34	9.62±2.8	−32.38±0.12	9.69±1.2	157.31±1.03	3.66±0.03	−0.51±0.12	104.59±0.14	0.63±0.11
6.98	13.93±0.73	11.64±3.1	−32.25±0.19	10.26±3.2	156.81±1.42	3.67±0.04	−0.57±0.15	104.59±0.27	0.64±0.14

on whether we started with the high- or the low-oxygen concentration parameters, showing that we have found the correct set of parameters. The resulting CEF parameters are listed in Table II. The CEF parameters determined for $ErBa_2Cu_3O_x$ are found to vary considerably as a function of oxygen content x, which is quantitatively discussed in Sec. VI.

V. MAGNETIC PROPERTIES

The CEF parameters may now be used to calculate the magnetic properties of $ErBa_2Cu_3O_x$. The magnetic single-ion susceptibility turns out to be extremely anisotropic, with the y axis as the easy axis of magnetization in agreement with the results of a neutron-diffraction study of the long-range antiferromagnetic ordering in $ErBa_2Cu_3O_x$.[21] As shown in Fig. 8, the magnetization calculations are in very good agreement with high-field magnetization measurements on a powder sample.[22] On the other hand, they deviate by typically 30% from single-crystal measurements,[23] which is most likely due to incomplete field penetration. Nevertheless, the high anisotropy between the in-plane and out-of-plane components observed in bulk magnetization measurements is well reproduced. The zero-field moment at saturation is drastically reduced below the free ion value of $9\mu_B$. For $ErBa_2Cu_3O_{6.98}$ the calculation yields $4.19\mu_B$, which favorably agrees with the Mössbauer value of $4.2\pm0.1\mu_B$ (Ref. 24) and to a lesser extent with the diffraction value of $4.8\pm0.2\mu_B$.[21] The calculated change of the magnetic moment between the $x=6.98$ and $x=6.09$ samples is $0.34\mu_B$. While this result agrees perfectly with the Mössbauer values,[24] it is in disagreement with diffraction measurements, which yield a reduction of $1.1\mu_B$ between $x=7$ and $x=6.5$.[21]

The comparison with heat-capacity measurements offers another possibility to check the reliability of the CEF parameters determined in the present work. A very detailed study was performed by van der Meulen *et al.*[25] and by Dunlap *et al.*[26] Some of their results are shown in Fig. 9 together with our calculations, which are in excellent agreement. Particularly, the shape of the Schottky anomaly in a field of 5 T is nicely reproduced. This anomaly originates from the splitting of the Kramers doublet ground state in the presence of a magnetic field.

VI. DISCUSSION

Equation (5) shows that the CEF parameters are functions of both the structure and the charge distribution. The point-charge approximation, however, has severe shortcomings and often provides physically unrealistic ligand charges Z. This is due to effects such as screening, shielding, antishielding, and covalent bonding. To overcome these problems, we proceed in two steps.

(1) Since we have shown previously that we can restrict our considerations to the nearest-neighbor oxygen shell, Eq. (5) transforms then into

$$A_{2n}^{2m}(x) = e|e|\langle r^{2n}\rangle Z(\mathrm{O}(2),\mathrm{O}(3))\gamma_{2n}^{2m}(x) \ . \tag{8}$$

The geometrical factors $\gamma_{2n}^{2m}(x)$ depend on the O(2) and O(3) positions.

(2) Considering relative changes of the CEF parame-

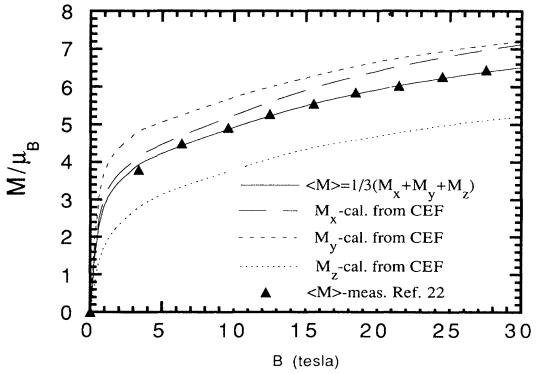

FIG. 8. Observed and calculated magnetization curve of $ErBa_2Cu_3O_{6.98}$.

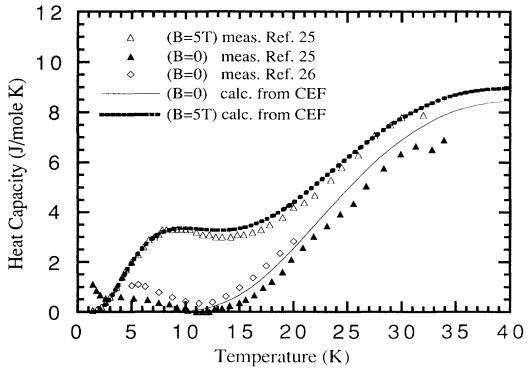

FIG. 9. Observed and calculated Schottky anomaly of the heat capacity of $ErBa_2Cu_3O_{6.98}$.

ters, we obtain from Eq. (8), assuming only structural modifications:

$$\frac{A_{2n}^{2m}(x)}{A_{2n}^{2m}(7)}=\frac{\gamma_{2n}^{2m}(x)}{\gamma_{2n}^{2m}(7)}\approx\left[\frac{\mathbf{r}-\mathbf{R}(7)}{\mathbf{r}-\mathbf{R}(x)}\right]^{2n+1}\leq 1 \quad \text{for } 6\leq x\leq 7 \ . \tag{9}$$

Since under a decrease of the oxygen content x the distances R-O(2) and R-O(3) are increasing (see Table I and Ref. 11), we expect a decrease of all the CEF parameters as a function of decreasing oxygen content x.

Figure 10 shows the observed and expected changes of the CEF parameters A_4^0, A_4^4, A_6^0, and A_6^4. Obviously the observed CEF values behave very differently from the values extrapolated according to Eq. (9). The nicest example is obtained by the behavior of the parameter A_4^0. While the structure parameters are increasing with decreasing oxygen content, the value of the CEF parameter A_4^0 increases, in total contradiction with any structural expectation. This means that structural considerations alone are not sufficient to reproduce these changes. An increase of the charge $Z(\mathrm{O}(2),\mathrm{O}(3))$ upon reduction of the sample could act as a compensation of the structural effects. This is consistent with the idea of charge transfer mentioned by Cava *et al.*,[10] since an increase of the electronic charge $Z(\mathrm{O}(2),\mathrm{O}(3))$ may be interpreted as a decrease of the hole concentration in the CuO_2 planes. In order to quantify these results we consider the point-charge relation

$$A_{2n}^{2m}(x)=e|e|\langle r^n\rangle Z(\mathrm{O}(2),\mathrm{O}(3))[1+\delta(x)]\gamma_{2n}^{2m}(x) \ , \tag{10}$$

where $\delta(x)$ describes the relative charge transfer. Taking the compound $ErBa_2Cu_3O_{6.98}$ as a reference [i.e., $\delta(6.98)=0$], a quantitative estimate of the actual charge transfer $Z(\mathrm{O}(2),\mathrm{O}(3))|e|\delta(x)$ can be obtained from Eq. (10):

$$A_{2n}^{2m}(x)/A_{2n}^{2m}(7)=[1+\delta(x)]\gamma_{2n}^{2m}(x)/\gamma_{2n}^{2m}(7) \ . \tag{11}$$

Since $\gamma_{2n}^{2m}(x)$ is known from crystallographic measurements and $A_{2n}^{2m}(x)$ from CEF spectroscopy, it is very easy to determine $\delta(x)$. We treated in this way only the leading fourth- and sixth-order parameters, since the second-order parameters are long-range parameters and the statistical uncertainty of the remaining orthorhombic parameters is rather large. In Fig. 11 we plot the resulting charge transfer $\langle Z|e|\delta(x)\rangle_{mn}$ as a function of the oxygen concentration x [assuming $Z(\mathrm{O}(2),\mathrm{O}(3))=-2$]. We find that a charge of 0.07 $|e|$/O is transferred into the planes when going from $x=6$ to $x=7$, which means that about 28% of the created holes go into the planes. This is slightly less than the value of 40% derived from resistivity measurements,[27] and slightly more than the charge transfer 0.04 $|e|$/O (0.08 $|e|$/Cu) derived from diffraction data by means of the bond valence sum formalism[10] for the related Y 1:2:3 compound (see Fig. 11). Our results show a linear dependence of the charge transferred as a function of x, in contrast to Cava *et al.*[10] who deduce a close relation between the two-plateau structure of T_c and the charge transfer with a pronounced discontinuity at $x\approx 6.4$. In the bond valence sum formalism a (non-)linear charge transfer is a direct consequence of a (non-)linear decrease of the cell parameter c with increasing x. In this respect the data by Cava *et al.*[10] are at variance with recent diffraction work published by Radaelli *et al.*,[28] who observed a linear relation between the

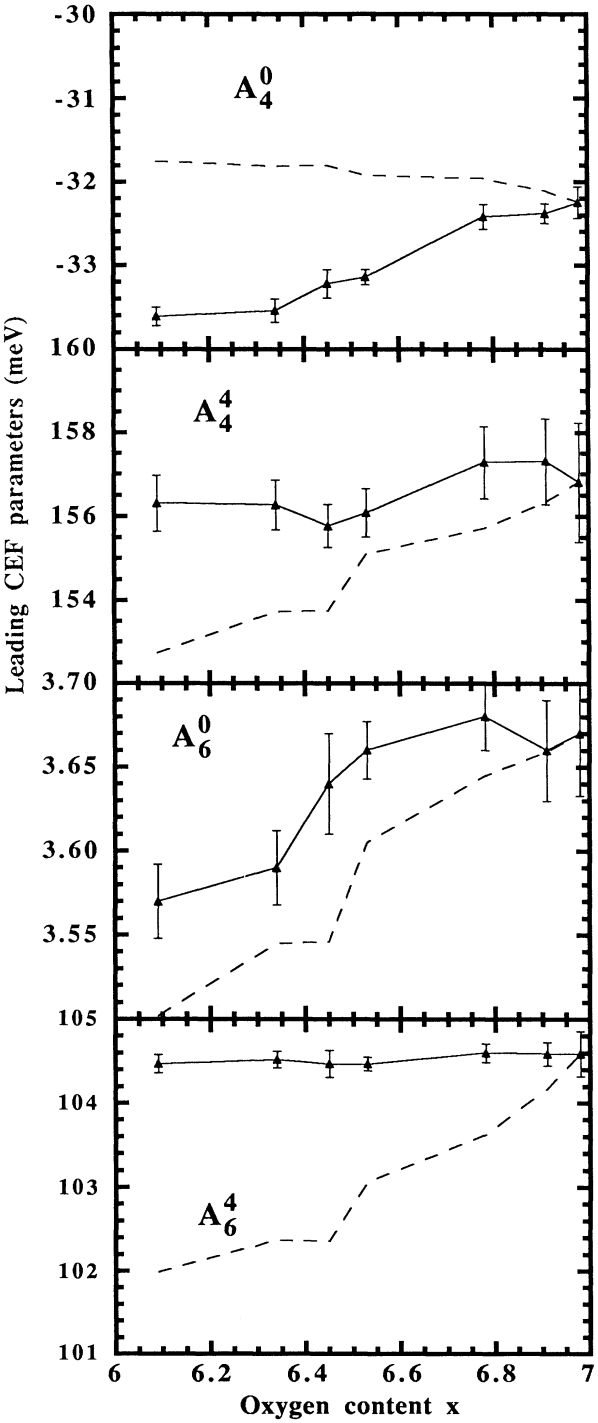

FIG. 10. Leading fourth- and six-order CEF parameters determined for $ErBa_2Cu_3O_x$ in the present work (triangles and solid curves). The values extrapolated from the structural changes alone are indicated by the dashed curves.

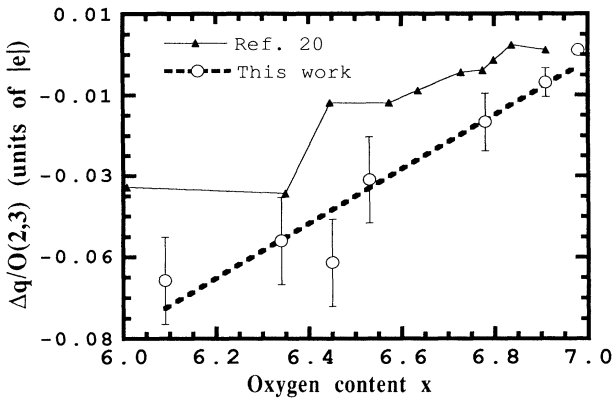

FIG. 11. Charge transfer vs oxygen content x derived for $ErBa_2Cu_2O_x$ in the present work, in comparison with the results obtained for $YBa_2Cu_3O_x$ from bond valence sum considerations. (Ref. 10)

lattice parameter c and the oxygen concentration x for $ErBa_2Cu_3O_x$ ($6<x<7$), which nicely supports the results of our CEF analysis.

VII. CONCLUSION

We have presented the results of inelastic neutron-scattering measurements of the CEF transitions of Er^{3+} in $ErBa_2Cu_3O_x$ for seven different oxygen concentrations. The determination of the CEF parameters, evaluated in the intermediate coupling approximation including J mixing, allows one to calculate several thermodynamic properties, which are in excellent agreement with experimental data. The comparison of the field-dependent properties turned out to be particularly useful, since the external field predominantly probes the ground-state wave functions of the CEF states.

The variation of CEF parameters with oxygen stoichiometry is shown to be the consequence of a linear charge transfer from the chains to the planes. We find that the decrease of T_c from 90 to 60 K is associated with a charge transfer of the order of 0.04 e/O, while an additional transfer of 0.03 e/O is needed to reach the insulating state. This type of analysis has been applied to other systems, such as $HoBa_2Cu_3O_x$ (Ref. 29) and $Nd_{2-x}Ce_xCuO_4$ (Ref. 30), where similar results were found.

In the present work we have analyzed the observed energy spectra in an integral manner, i.e., we have not considered deviations from an ideal crystal structure which, however, is known to be distorted particularly upon variation of the oxygen content from $x=6$ to $x=7$. Deviations from this ideal case are certainly reflected in the anomalous linewidth behavior of the lowest-lying CEF transition A, as mentioned in Sec. III. Indeed, a detailed analysis shows that this transition is composed of a superposition of three components whose spectral weights distinctly depend on the oxygen content x. With the CEF interaction being a local probe, there is no doubt that these substructures originate from different local environments of the Er^{3+} ions, which obviously coexist in the compound $ErBa_2Cu_3O_x$. Similar effects have been observed for $ErBa_2Cu_3O_x$ in the composition range $6.25<x<6.45$.[28] We interpret the three components in terms of local regions of either semiconducting or metallic character. The superconductivity can then be shown to result from the formation of a two-dimensional percolative network. As a consequence the two-plateau structure of T_c is closely related to the variation of the proportions of each component versus the oxygen content x. A preliminary account of these ideas will be published elsewhere.[31]

Note added in proof. Recently, an independent inelastic-neutron-scattering study of the crystalline electric field in $ErBa_2Cu_3O_7$ was reported by L. Soderholm, C.-K. Loong, and S. Kern in Phys. Rev. B **45**, 10062 (1992). Our results obtained for $ErBa_2Cu_3O_{6.98}$ as described in Sec. III A are consistent with the data obtained by Soderholm, Loong, and Kern.

ACKNOWLEDGMENTS

Financial support by the Swiss National Science Foundation is gratefully acknowledged. One of us (J.M.) would like to thank the Institute for Metal Physics, Ekaterinburg, Russia, for the hospitality in connection with the dc susceptibility measurements.

*Author to whom correspondence may be sent: Joël Mesot, Laboratory for Neutron Scattering, ETH Zurich, CH-5232 Villigen PSI, Switzerland; Email: Mesot CAGEIR5A.

[1]F. Hulliger and H. R. Ott, Z. Phys. B **68**, 291 (1987).

[2]S. M. Green, C. Jiang, H. J. Luo, Y. Mei, and C. Politis, Physica C **153-155**, 182 (1988).

[3]R. A. M. van Woerden, H. J. Terpstra, C. F. van Bruggen, M. Kroan, and D. M. de Leeuw, Physica C **170**, 112 (1990).

[4]See, for example, *Electronic Properties of High-T_c Superconductors and Related Compounds,* edited by H. Kuzmany, M. Mehring, and J. Fink (Springer, Berlin, 1990), Vol. 99.

[5]J. W. Lynn, T. W. Clinton, W.-H. Li, R. W. Erwin, J. Z. Liu, K. Vandervoort, and R. N. Shelton, Phys. Rev. Lett. **50**, 2606 (1989).

[6]P. Allenspach, A. Furrer, and F. Hulliger, Phys. Rev. B **39**, 2226 (1989).

[7]E. A. Goremychkin, R. Osborn, and A. D. Taylor, Pis'ma Zh. Eksp. Teor. Fiz. **50**, 351 (1989) [JETP Lett. **50**, 380 (1989)].

[8]A. Furrer, P. Allenspach, J. Mesot, U. Staub, H. Blank, H. Mutka, C. Vettier, E. Kaldis, J. Karpinski, S. Rusiecki, and A. Mirmelstein, Eur. J. Solid State Inorg. Chem. **28**, 627 (1991).

[9]L. Soderholm, C.-K. Loong, G. L. Goodman, and B. D. Dabrowski, Phys. Rev. B **43**, 7923 (1991).

[10]R. J. Cava, A. W. Hewat, E. A. Hewat, B. Battlog, M. Marezio, K. M. Rabe, J. J. Krajewski, W. F. Peck, Jr., and L. W. Rupp, Jr., Physica C **165**, 419 (1990).

[11]B. Rupp, E. Pörschke, P. Meuffels, P. Fischer, and P. Allenspach, Phys. Rev. B **40**, 4472 (1989).

[12]G. T. Trammel, Phys. Rev. **92**, 1387 (1953).

[13]A. J. Freeman and J. P. Desclaux, J. Magn. Magn. Mater. **12**, 11 (1979).

[14]B. R. Judd, *Operator Techniques in Atomic Spectrscopy* (McGraw-Hill, New York, 1963).

[15]M. T. Hutchings, in *Solid State Physics,* edited by F. Seitz and D. Turnbull (Academic, New York, 1964), Vol. 16, p. 227.
[16]B. J. Wybourne, J. Chem. Phys. **32**, 639 (1960).
[17]C. W. Nielson and G. F. Koster, *Spectroscopic Coefficients for the p^n, d^n, and f^n Configurations* (MIT, Cambridge, MA, 1964).
[18]A. Furrer, P. Brüesch, and P. Unternährer, Phys. Rev. B **38**, 4616 (1988).
[19]V. Nekvasil, Solid State Commun. **65**, 1103 (1988).
[20]K. R. Lea, M. J. M. Leask, and W. P. Wolf, J. Phys. Chem. Solids **23**, 1381 (1962).
[21]H. Maletta, E. Pörscke, T. Chattopadahyay, and P. J. Brown, Physica C **166**, 9 (1990).
[22]L. W. Roeland, F. R. De Boer, Y. K. Huang, A. A. Menovsky, and K. Kadowaki, Physica C **152**, 72 (1988).
[23]M. Guillot, J. L. Tholence, A. Marchand, G. Chouteau, M. Potel, P. Gougeon, H. Noel, and J. C. Levet, Physica B **155**, 140 (1989).
[24]J. A. Hodges, P. Imbert, J. B. Marimon de Cunha, and J. P. Sanchez, Physica C **160**, 49 (1989).
[25]H. P. Van Der Meulen, J. J. M. Franse, Z. Tarnawaki, K. Kadowaki, J. C. P. Klasse, and A. A. Menovski, Physica C **152**, 65 (1988).
[26]B. D. Dunlap, M. Slaski, D. G. Hinks, L. Soderholm, M. Beno, K. Zhang, C. Segre, G. W. Crabtree, W. K. Kwok, S. K. Malik, I. K. Schuller, J. D. Jorgensen, and Z. Sungaila, J. Magn. Magn. Mater. **68**, L139 (1987).
[27]U. Welp, S. Fleshler, W. K. Kwok, J. Downey, Y. Fang, G. W. Crabtree, and J. Z. Liu, Phys. Rev. B **42**, 10 189 (1990).
[28]P. G. Radaelli, C. U. Segre, D. G. Hinks, and J. D. Jorgensen, Phys. Rev. B **45**, 4923 (1992).
[29]U. Staub, P. Allenspach, J. Mesot, A. Furrer, H. Blank, and H. Mutka, Physica B **180-181**, 417 (1992).
[30]A. Furrer, P. Allenspach, J. Mesot and U. Staub, Physica C **168**, 609 (1990).
[31]J. Mesot, P. Allenspach, U. Staub, A. Furrer, and H. Mutka, Phys. Rev. Lett. **70**, 865 (1993).